PAPER

Hyperparameter-tuned prediction of somatic symptom disorder using functional near-infrared spectroscopy-based dynamic functional connectivity

Journal of Neural Engineering

PAPER

Hyperparameter-tuned prediction of somatic symptom disorder using functional near-infrared spectroscopy-based dynamic functional connectivity

RECEIVED
22 May 2019

REVISED
22 October 2019

ACCEPTED FOR PUBLICATION
23 October 2019

PUBLISHED
16 December 2019

Aykut Eken[1,2,6], **Burçin Çolak**[3], **Neşe Burcu Bal**[4], **Adnan Kuşman**[3], **Selma Çilem Kızılpınar**[3], **Damla Sayar Akaslan**[3] **and Bora Baskak**[3,5]

[1] ICFO-Institut de Ciències Fotòniques Barcelona Institute of Science and Technology, Castelldefels, Barcelona, Spain
[2] Center for Brain and Cognition, Pompeu Fabra University, Barcelona, Spain
[3] Faculty of Medicine, Department of Psychiatry, Ankara University, Ankara, Turkey
[4] Department of Psychiatry, Health Sciences University, Istanbul, Turkey
[5] Ankara University, Brain Research and Application Center, Ankara, Turkey
[6] Author to whom any correspondence should be addressed.

E-mail: aykut.eken@icfo.eu

Keywords: somatic symptom disorder, fNIRS, machine learning, dynamic functional connectivity, hyperparameter optimization

Abstract

Objective. Somatic symptom disorder (SSD) is a reflection of medically unexplained physical symptoms that lead to distress and impairment in social and occupational functioning. SSD is phenomenologically diagnosed and its neurobiology remains unsolved. *Approach.* In this study, we performed hyper-parameter optimized classification to distinguish 19 persistent SSD patients and 21 healthy controls by utilizing functional near-infrared spectroscopy via performing two painful stimulation experiments, individual pain threshold (IND) and constant sub-threshold (SUB) that include conditions with different levels of pain (INDc and SUBc) and brush stimulation. We estimated a dynamic functional connectivity time series by using sliding window correlation method and extracted features from these time series for these conditions and different cortical regions. *Main results.* Our results showed that we found highest specificity (85%) with highest accuracy (82%) and 81% sensitivity using an SVM classifier by utilizing connections between right superior temporal–left angular gyri, right middle frontal (MFG)—left supramarginal gyri and right middle temporal—left middle frontal gyri from the INDc condition. *Significance.* Our results suggest that fNIRS may distinguish subjects with SSD from healthy controls by applying pain in levels of individual pain-threshold and bilateral MFG, left inferior parietal and right temporal gyrus might be robust biomarkers to be considered for SSD neurobiology.

1. Introduction

Somatoform disorders are characterized by the presence of physical symptoms that suggest a general medical condition that are not fully explained by a general medical condition, by the direct effects of a substance, or by another mental disorder. According to the 5th version of diagnostic and statistical manual of mental disorders (DSM-5) (American Psychiatric Association 2013) the somatoform disorder definition was replaced by 'somatic symptom and related disorders' and encompasses a group of disorders such as somatic symptom disorder (SSD), illness anxiety disorder and conversion disorder. Particularly, the persistent SSD diagnosis requires the existence of somatic symptoms accompanied by excessive thoughts, feelings or behaviors related with somatic symptoms that endure more than six months. According to the DSM-5, in order to meet the diagnostic criteria, the symptoms must lead to clinically significant distress in daily life or impairment in social, occupational, or other areas of functioning.

Epidemiologically, the prevalence of SSD is estimated as 5%–7% in the general population (American Psychiatric Association 2013) and increases up to 17% in primary care admissions (Kurlansik and Maffei 2016). The economic burden is also devastating. This group of disorders are associated with a high economic

cost not only by the overutilization of the health care system (Barsky *et al* 2005), but unemployment and early retirement rates as well as absenteeism from work are also considerably high (Konnopka *et al* 2013). In spite of this economic burden, the current diagnosis of these disorders solely depends on direct observation of symptoms and underlying neurobiology is not clear. Cognitive alterations in perception and processing an attribution of pain have been proposed (Barsky *et al* 1988), and structural and functional neuroimaging studies revealed some of the underlying neural circuits. In an fMRI study, it was showed that patients display increased activity as a response to painful stimuli in known pain processing regions such as the thalamus, basal ganglia, operculo-insular cortex as well as the prefrontal and temporal cortices (Stoeter *et al* 2007). In another study, Yoshino and colleagues found evidence regarding higher activity during resting state in the precentral gyrus, which is also an element of the pain network (Yoshino *et al* 2014). Browning and colleagues reviewed neuroimaging studies in somatoform disorders and concluded that when compared with non-clinical groups, somatoform diagnoses are associated with increased activity of limbic and cortical regions in response to painful stimuli and a generalized decrease in gray matter density (Browning *et al* 2011). But a great majority of these studies enrolled subjects with a former definition of somatoform pain disorder and fibromyalgia where the prominent symptom was pain. Very few studies of patients with a former diagnosis of 'somatization disorder' with a range of somatic symptoms have been published that reported anomalies in resting activation (Garcia-Campayo *et al* 2001, Hakala *et al* 2006) and some structural differences (Hakala *et al* 2004). Browning and colleagues commented that published studies in somatization disorders involve small samples (maximum $n = 11$, with similar cohorts of patients repeatedly analyzed in different studies) and therefore clear conclusions cannot be drawn about the patterns of activation associated with this diagnosis (Browning *et al* 2011). Ever since that review, literature surveys fail to identify a functional neuroimaging study that evaluates the response to painful stimuli in subjects with a persistent somatic symptom disorder. Another review that focuses on functional somatic syndromes showed that central sensitization might be a common indicator for them (Bourke *et al* 2015).

The vast majority of the studies conducted on somatoform disorders were performed using functional magnetic resonance imaging (fMRI). However, fMRI has several limitations compared with other neuroimaging modalities, such as being expensive, a noisy scanner, with strict restrictions of motion and a stressful environment that may cause several false positive activations (Scarapicchia *et al* 2017) particularly in psychiatric populations (Baskak 2018). fNIRS is a relatively new imaging technology capable of measuring cortical activity and can be simultaneously used with EEG (Dutta *et al* 2015, Koo *et al* 2015, Peng *et al* 2016, Chiarelli *et al* 2017, 2018, Kassab *et al* 2018). To perform experiments using fNIRS in a more naturalistic environment is more possible than using fMRI (Rolfe 2000). Since fNIRS is relatively insensitive to motion artifacts, subjects can be examined in a natural sitting position, without any surrounding distraction (Takizawa *et al* 2008). fNIRS may especially be suitable for subjects with SSD who may be sensitive to physical restriction and discomfort associated with the MRI environment. There is some indirect evidence that the MRI environment leads to significant changes in the hypothalamo-pituiatary-adrenal axis (Tessner *et al* 2006), a system which is found disturbed in subjects with functional somatic symptoms (Janssens *et al* 2012).

Several techniques adopted from machine learning approaches have been utilized in neuroimaging for the classification of several pain related psychiatric disorders (see reviews (Davis *et al* 2017, Lotsch and Ultsch 2018)). In detail, these algorithms were successfully employed for the classification of subjects with fibromyalgia (Sundermann *et al* 2014, Robinson *et al* 2015, Lopez-Sola *et al* 2017, Gokcay *et al* 2018) as well as chronic back pain (Callan *et al* 2014, Lee *et al* 2018, Mano *et al* 2018).

We aimed to examine cortical activity in response to painful stimuli in subjects with DSM-5 persistent SSD with fNIRS. We tried to predict membership to the SSD diagnostic category with sufficient sensitivity and accuracy by using features extracted from fNIRS signals acquired after an experimental task that includes painful and non-painful stimulation. Here it is important to note that as with most psychiatric diagnoses, current diagnosis of SSD is made by assessing clusters of symptoms in a psychiatric interview and our aim is not to test a costly neuro-imaging-based alternative. However, construct validity of psychiatric diagnoses is of great concern (Jablensky 2016) and neurophysiologic measures including functional neuroimaging are proposed to test the validity of these disorders by investigating possible biomarkers that may help to reveal the true neurobiology behind these (Andreasen 1995, Linden and Fallgatter 2009) disorders. We accordingly aimed (i) to assess robust, task-specific and region-based biomarker/s for SSD by using fNIRS, and (ii) to create a hyperparameter-tuned machine learning model by using these biomarkers that maximize the accuracy, sensitivity and specificity.

2. Methods

2.1. Participants

The index group comprised 19 consecutive outpatients with SSD. Participants were evaluated by two experienced psychiatrists and those diagnosed with DSM-5 persistent SSD were invited to participate. Inclusion criteria were (i) age between 18–65, (ii) being predominantly right-handed, (iii) willing to participate in the study. Subjects with (i) a major

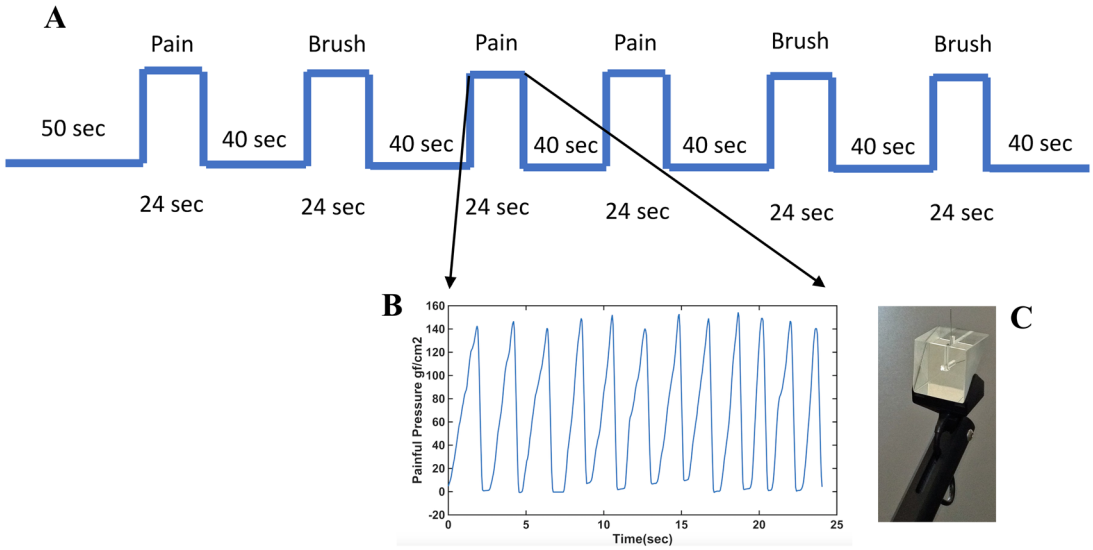

Figure 1. Experimental design representation for SUB and IND. (a) Experimental block design. (b) Painful stimulation in one pain condition. In this graph, the waveform represents a constant sub-threshold painful stimulation (SUBc) for 24 sec. (c) Electronic Von-Frey anesthesiometer that was used for painful stimulation application.

depressive episode (ii) history of neurological disorders, (iii) a chronic general medical condition, (iv) head trauma (resulting in loss of consciousness longer than 30 min), as well as (v) alcohol and/or substance use disorder (except tobacco) were excluded. Depression and SSD are highly comorbid disorders and although we excluded clinically established cases of depression, sub-clinical depressive symptoms may also interfere with the cortical processing of pain (Vossen *et al* 2006, Strigo *et al* 2008, Rodriguez-Raecke *et al* 2014). We therefore applied Beck Depression Inventory (BDI) (Hisli 1998) and subjects with BDI scores over 30 that correspond to depressive symptoms above a moderate level were also excluded ($N = 11$). Thus, the index group was composed of the remaining 19 subjects. The control group consisted of 21 healthy participants who were also evaluated by two experienced psychiatrists in order to rule out the existence or history of a psychiatric disorder and psychotropic drug use. Inclusion and exclusion criteria were the same as the index group. Handedness was assessed with the Edinburgh Handedness Inventory (Oldfield 1971). All participants stopped the intake for analgesic drugs at least 48 h before the experiment. They were also informed about the protocol that was approved by the Ankara University Ethical Board Committee (No. 04-240-18). The protocol was performed according to the Helsinki declaration and subjects signed informed consent before participation.

2.2. Pain threshold measurement

Pain threshold measurement was performed by applying quantitative sensory testing (QST) method via an electronic Von Frey (eVF) aesthesiometer (Ugo Basile Co, Italy) as previously published (Vivancos *et al* 2004, KuKanich *et al* 2005, Ambalavanar *et al* 2006, Tena *et al* 2012). We applied eVF five times on the right thumb of every participant and they were asked to give a verbal response as soon as they feel unpleasant. After these five measurements, we calculated the average of these measurements and the result was recorded as the individual mechanical pain threshold.

2.3. Experimental design

We conducted two different painful stimulation experiments by using eVF to apply painful stimuli (i) at a constant sub-threshold level (SUB) and (ii) at the individual pain threshold level (IND). In both experiments, we also performed brush stimulation (BS) as the control condition. In the BS condition, we used a toothbrush and applied it manually to the thumb 24 times during the stimulation period. In the SUB experiment during the painful stimulation condition (SUBc), a constant painful stimulus (130 gf cm^{-2}) and in the IND experiment during painful stimulation condition (INDc) stimulus at the individual pain threshold that was calculated for each individual was applied. After a 50 s resting period, we applied 24 s of painful stimulation and a 40 s resting period as three trials and 24 s of brush stimulation with a 40 s resting period as three trials. The experimental design is illustrated in figure 1(a). While performing INDc and SUBc, the applicant applied the painful stimulation 12 times during 24 s. In figures 1(b) and (c), painful stimulation for one trial and eVF are shown respectively. After every painful stimulus trial, we applied the Visual Analog Scale (VAS) to the participant to rate the pain intensity between 0–100.

2.4. fNIRS system

In our study, fNIRS experiments were carried out at Ankara University Brain Research Center (AÜBAUM) with a Hitachi ETG-4000 continuous wave (CW) fNIRS system (Hitachi Co., Japan). Optical near-infrared

light with two different wavelengths (695 and 830 nm) were sent to the head surface via a source optode and captured back by a detector optode. We used the 3 × 11 optode configuration including 52 channels. Source–detector distances were 2.5 cm. Sampling frequency was 10 Hz.

2.5. Probe positioning

While positioning the probe on the scalp, we utilized the EEG 10–20 system to place the probe set. Due to performing a painful stimulation experiment, we focused on placing probes around the postcentral gyrus that correspond to the C3 and C4 channels in EEG 10–20 systems according to the previous studies (Okamoto *et al* 2004, Koessler *et al* 2009). In this system, 50% of the distance from nasion to inion corresponds to the channel Cz. After defining the position of Cz, we set the 3 × 11 probe holders for each hemisphere over the line passing through both ears. C3 and C4 electrode positions were defined by measuring the distance between both tragi, and 30% of this value gave us the position of C3 from the left tragus and C4 from the right tragus, which corresponded to the left and right SI, respectively. Detector numbers 17 and 22 were placed onto the C3 and C4 electrode positions that correspond to the left and right postcentral gyrus according to the previous studies. After positioning the probe holder, we marked source and detector positions by using a 3D digitizer (Polhemus Co., Vermont) to determine the exact position of each channel in a further step. After acquiring the position file, we utilized it for spatial registration to the Montreal Neurological Institute (MNI) template to determine the corresponding landmarks using the NIRS analysis package (Fekete *et al* 2011). Then, we averaged coordinate values of all participants (Asano *et al* 2004). To obtain brain regions corresponding to MNI coordinates, we used the LONI Probabilistic Brain Atlas (LPBA 40) (Shattuck *et al* 2008). Channel configuration on the head is shown in figure 2. Channel numbers and corresponding cortical regions with average MNI coordinates are shown in table 1.

2.6. Data analysis

We first converted our optical density time series to concentration changes of an oxy-hemoglobin (ΔHbO_2) and de-oxyhemoglobin (ΔHb) time series by using the modified Beer–Lambert law (Cope and Delpy 1988). After this procedure, we performed preprocessing to ΔHbO_2 and ΔHb signals and performed a region of interest (ROI) analysis using only channel information and ΔHbO_2 due to having higher SNR than ΔHb (Homae *et al* 2010, Zhang *et al* 2010, Niu *et al* 2011, Montero-Hernandez *et al* 2018) and it was more associated with CBF than ΔHb was (Strangman *et al* 2002). We performed sliding window correlation (SWC) (Sakoglu *et al* 2010) that was previously used in fNIRS (Li *et al* 2015) to obtain dynamic functional connectivity (dFC) changes by using the time series in regions. After extracting dFC changes and averaging them according to the different conditions, INDc, SUBc and BS, mean averaged dFC values were used to create a feature vector for these conditions. Among these extracted features, we selected the most discriminative features by using least absolute shrinkage and selection operator (LASSO). Finally, we performed classification by using these features and utilizing different classification methods with defined optimum hyperparameters via Bayesian optimization. Our whole data analysis procedure is shown in figure 3.

2.6.1. *fNIRS preprocessing*

We used MATLAB (MathWorks, Inc., Natick, Massachusetts) for the preprocessing of ΔHbO_2 data. The preprocessing pipeline included baseline correction, detrending to eliminate low frequency drift, filtering for the removal of physiological confounding effects and motion artifacts and the averaging of blocks in the same condition. First, we performed baseline correction by removing the mean of whole time series for every channel. Then, we removed the very low frequency global drift (<0.01 Hz) by using wavelet-based minimum description length detrending (Jang *et al* 2009). To remove the physiological confounding effects, such as Mayer waves, respiration and heartbeat, we performed a 0.01–0.1 Hz second-order Butterworth band-pass filter. After these preprocessing steps, we visually checked the whole time series and performed motion artifact removal using wavelet filtering (Molavi and Dumont 2012). We used Daubechies 6 (db6) wavelet to remove the motion artifacts.

2.6.2. *Region of interest (ROI) analysis*

After the preprocessing steps, we averaged the ΔHbO_2 time series in channels that correspond to the same region according to the LONI probabilistic atlas for every subject. After mapping the channels to this atlas, we reduced our 52 channels up to 20 bilateral regions. Among these 20 bilateral regions, we only excluded bilateral middle occipital gyrus from analysis due to less relevance with pain perception in SSD (Stoeter *et al* 2007, Gundel *et al* 2008) and also for the resting-state functional connectivity studies (Su *et al* 2014, Song *et al* 2015). The remaining 18 regions are the bilateral angular gyrus (AG), superior parietal gyrus (SPG), supramarginal gyrus (SMG), pre central gyrus (PreCG), post central gyrus (PostCG), middle frontal gyrus (MFG), superior frontal gyrus (SFG), middle temporal gyrus (MTG) and superior temporal gyrus (STG). An example of our preprocessing and ROI analysis results are shown in figure 4.

2.6.3. *Identifying ideal features*

2.6.3.1. *Feature extraction using sliding window correlation*

After ROI analysis, we performed sliding window correlation (SWC) for every experiment and every

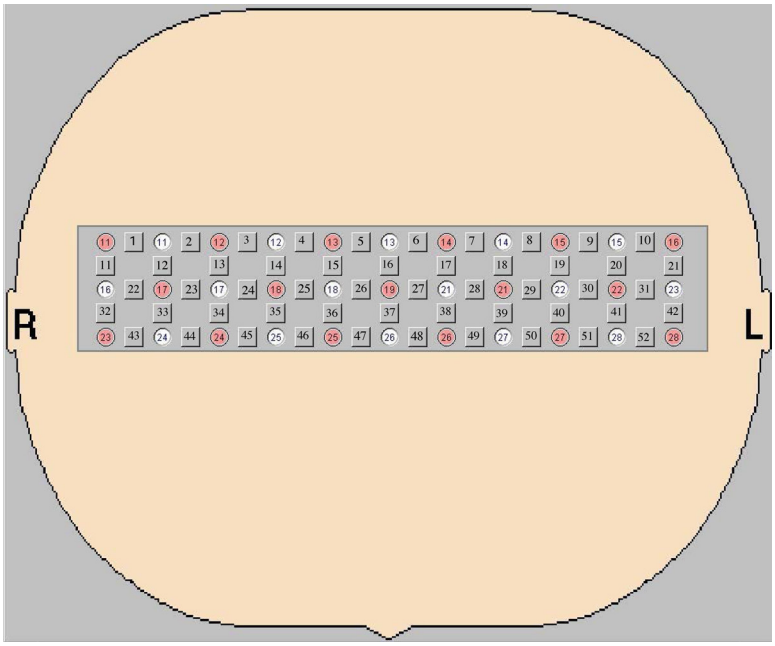

Figure 2. Channel and optode configuration of the 3 × 11 probe setting. In this figure, locations that are represented as squares are channels. White circles that include numbers in black are detectors. Red circles that include numbers in black are sources. R: right, L: left.

region to estimate the dynamic functional connectivity (dFC) maps. For dFC estimation, $r_{x,y}$ represents the correlation coefficients vector, x and y are the ΔHbO_2 signals for two different regions and i is the index. l and t represent the window size and index in this window $(t : l, l+1, l+2, l+3 \ldots..)$.

$$r_{xy}(l) = \frac{\sum_{i=t-l+1}^{t}(x_i - \bar{x}_i)(y_i - \bar{y}_i)}{\sqrt{\sum_{i=t-l+1}^{t}(x_i - \bar{x}_i)^2 \sum_{i=t-l+1}^{t}(y_i - \bar{y}_i)^2}}.$$

For this study, we chose time window 24 s that represents 240 samples. After obtaining the correlation vector r_{xy}, we performed trial extraction over this vector using the task waveform. We separately averaged the corresponding blocks for both brush and painful stimulation. After this block averaging, we estimated the mean value for both averaged trials. For 18 regions, we had an 18 × 18 connection matrix for all conditions. However, we only used the upper diagonal part by excluding the diagonal side. Therefore, we obtained 18 × 17/2 = 153 values for both painful and brush stimulation ΔHbO_2 responses. We applied this procedure for three different conditions (SUBc, INDc, BS) that we obtained from SUB and IND separately. Due to having BS conditions from both experiments, we averaged the BS values for every subject. Therefore, we obtained three feature vectors (SUBc, INDc, BS) that has dimensions of 40 × 153. Due to having values between [−1,1], we did not perform any normalization like z-score.

2.6.3.2. Feature selection using LASSO regression

After creating the feature vectors for three conditions, we utilized least absolute shrinkage and selection operator (LASSO) regression to find the most informative features among the 153 features (Tibshirani 1996). LASSO is a penalized regression method that estimates coefficient vector $\hat{\beta}$ and adds a penalty factor to these coefficients by performing L1 regularization. $\hat{\beta}$ is the coefficient vector that has the d number of features. y_i is the binomial response that represents SSD as 1 and HC as 0 and $x_i : (x_1, x_2, x_3 \ldots\ldots x_d)^T$ for the ith observation. N represents the number of observations. λ is a positive regularization parameter on the L1 penalty. Our objective function and penalty factor are defined as;

$$\min_{\hat{\beta}} \left\{ \frac{1}{N}\sum_{i=1}^{N} (y_i - x_i^T\hat{\beta})^2 + \lambda \sum_{j=1}^{d} |\beta_j| \right\}.$$

LASSO is an effective feature reduction method over datasets that has small sample size and high number of dimension (Zou and Hastie 2005). We performed LASSO with five-fold cross validation to obtain optimal λ with mean squared error criterion. According to this optimal λ value, we selected the features that their corresponding coefficients are non-zero. After performing LASSO, for INDc, connections between Right STG/Left AG, Right MFG/Left SMG, Right MTG/Left MFG, for the SUBc condition, connections between Left MFG/Left SPG, Left SFG/Left AG, Right AG/Left STG, for BS condition connections between Right SFG/Left PreCG, Right MFG/Left MFG, Right PostCG/Left STG were used as features for these three feature vectors. Therefore, we obtained three 40 × 3 feature vectors for INDc, SUBc and BS conditions. Connections used as features for all these conditions are shown in figure 5 and mean correlation vectors for these regions are shown in figure 6.

Table 1. Channel numbers and average coordinate positions with corresponding cortical structures registered onto MNI space after using LPBA 40 cortical atlas. Probability values were obtained from the LPBA 40 cortical atlas (L: left, R: right).

Channel number	Probability	Region	Mean *X*	Mean *Y*	Mean *Z*	Std. dev (mm).
1	0,93	R middle occipital gyrus	52	−75	22	14,26
2	1,00	R angular gyrus	54	−64	44	11,92
3	0,88	R angular gyrus	46	−54	60	9,09
4	1,00	R superior parietal gyrus	31	−48	73	6,85
5	0,83	R superior parietal gyrus	11	−45	79	5,89
6	0,69	L superior parietal gyrus	−12	−45	78	6,27
7	1,00	L superior parietal gyrus	−32	−49	71	6,64
8	0,78	L angular gyrus	−46	−56	58	8,25
9	0,97	L angular gyrus	−53	−68	41	11,21
10	0,98	L middle occipital gyrus	−51	−79	19	13,35
11	0,58	R middle occipital gyrus	60	−67	6	14,97
12	0,91	R angular gyrus	62	−56	32	12,36
13	0,64	R angular gyrus	58	−45	53	9,12
14	0,64	R superior parietal gyrus	42	−37	68	7,68
15	0,69	R postcentral gyrus	22	−31	77	4,81
16	0,34	R precentral gyrus	−1	−29	76	4,18
17	0,60	L postcentral gyrus	−25	−33	75	6,10
18	0,62	L superior parietal gyrus	−45	−39	65	6,90
19	0,67	L angular gyrus	−58	−49	49	9,19
20	0,93	L angular gyrus	−61	−61	26	12,15
21	0,60	L middle occipital gyrus	−57	−73	1	13,82
22	0,56	R middle temporal gyrus	68	−48	15	12,27
23	0,81	R supramarginal gyrus	67	−37	40	10,18
24	0,74	R supramarginal gyrus	54	−28	60	8,76
25	0,60	R precentral gyrus	33	−20	73	7,97
26	0,63	R precentral gyrus	10	−15	77	6,10
27	0,72	L precentral gyrus	−14	−16	78	6,96
28	0,69	L postcentral gyrus	−38	−23	71	7,16
29	0,74	L supramarginal gyrus	−56	−32	55	8,54
30	0,92	L supramarginal gyrus	−66	−42	34	11,17
31	0,82	L middle temporal gyrus	−66	−54	8	13,08
32	0,92	R middle temporal gyrus	71	−39	−5	13,46
33	0,50	R supramarginal gyrus	71	−27	22	11,12
34	0,86	R supramarginal gyrus	64	−17	46	9,36
35	0,53	R postcentral gyrus	45	−9	63	8,87
36	0,83	R superior frontal gyrus	21	−2	74	6,90
37	0,63	L superior frontal gyrus	−2	−1	73	6,40
38	0,61	L superior frontal gyrus	−26	−4	72	7,61
39	0,63	L postcentral gyrus	−49	−12	60	8,02
40	0,75	L supramarginal gyrus	−64	−22	41	9,88
41	0,91	L superior temporal gyrus	−69	−33	16	11,65
42	0,55	L middle temporal gyrus	−67	−45	−12	13,41
43	0,71	R superior temporal gyrus	71	−18	3	13,16
44	0,86	R postcentral gyrus	68	−8	29	11,35
45	0,82	R precentral gyrus	55	2	50	9,95
46	0,67	R middle frontal gyrus	34	9	65	8,52
47	1,00	R superior frontal gyrus	10	12	71	7,07
48	1,00	L superior frontal gyrus	−14	12	71	7,45
49	0,90	L middle frontal gyrus	−39	7	62	8,59
50	0,73	L precentral gyrus	−58	−3	45	9,50
51	0,77	L postcentral gyrus	−67	−13	22	10,96
52	0,90	L middle temporal gyrus	−70	−24	−4	12,23

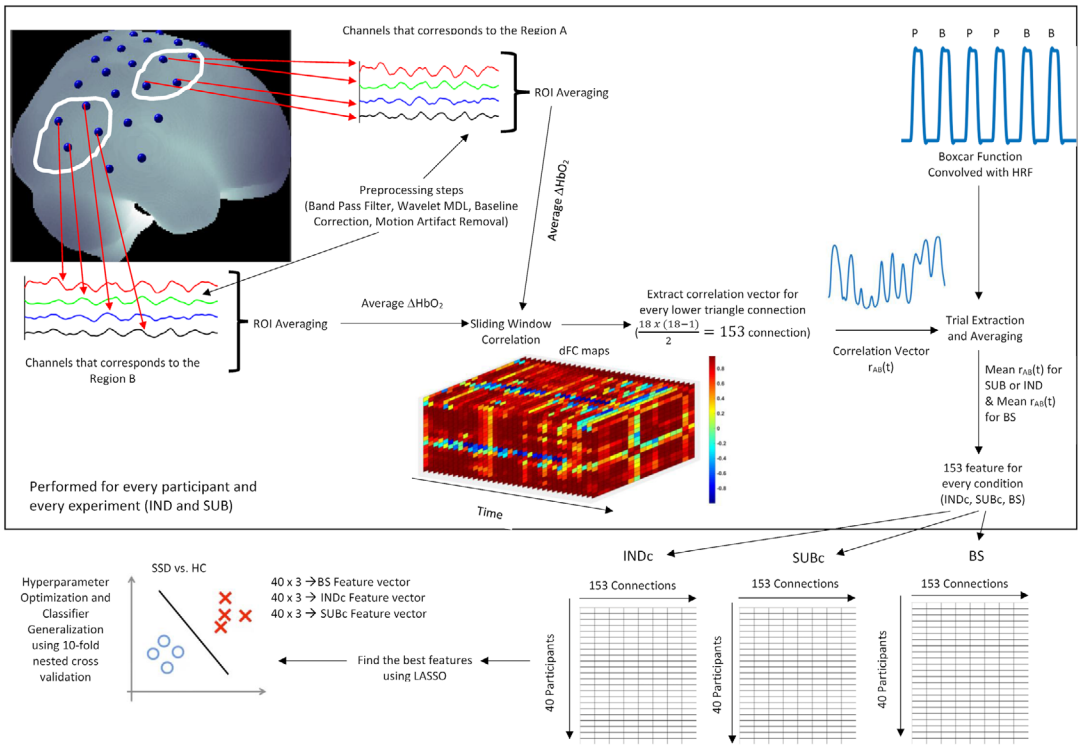

Figure 3. Data analysis procedure. In this diagram, after pre-processing and region of interest (ROI) analysis of two different regions (A) and (B), it was shown how to extract features. Dynamic functional connectivity was applied to estimate the correlation vector ($r_{AB}(t)$) to these regions by using sliding window correlation (SWC). Trial extraction and averaging was performed by utilizing boxcar function that includes related trials with pain (P) and brush (B) for both IND and SUB experiments. After trial extraction and averaging, we obtained mean $r_{AB}(t)$ for both SUBc or INDc and BS conditions. After performing this procedure for every participant and every region, least absolute shrinkage and selection operator (LASSO) was performed to find the best features for three different conditions and hyperparameter-tuned classification for SSD and HC was performed.

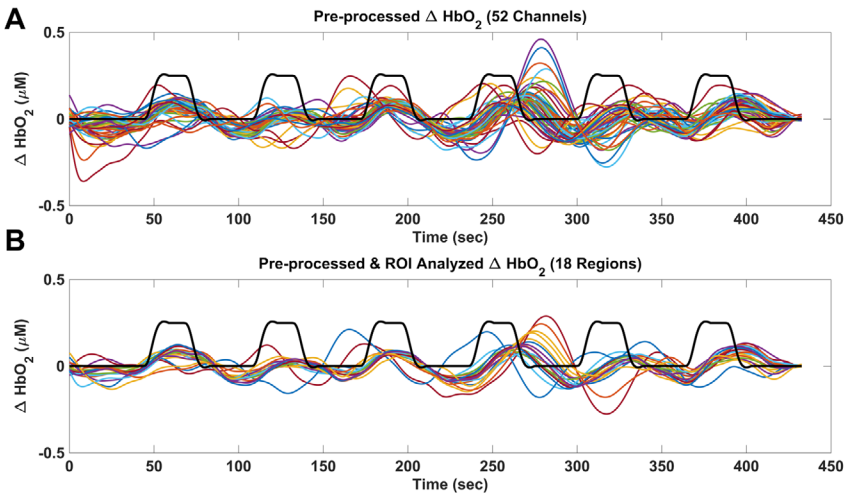

Figure 4. An example of preprocessing results (A) and its ROI analysis (B) of fNIRS signals of a healthy control participant. Black represents the HRF convolved boxcar function.

2.6.4. Hyperparameter optimization and classification
After the selection of most informative features for separate feature vectors of different conditions (INDc, SUBc, BS), due to having low number of features for both three feature sets, we performed the Bayesian optimization algorithm on the models that we trained by using these datasets to choose the best parameters that minimizes the validation loss. In this method, we call $\boldsymbol{\theta}$ the set of hyperparameters and $L(\boldsymbol{\theta})$ the validation loss function. Our objective is to find the $\boldsymbol{\theta}^*$ values that minimize this function.

$$\boldsymbol{\theta}^* = \arg\min_{\boldsymbol{\theta}} L(\boldsymbol{\theta}).$$

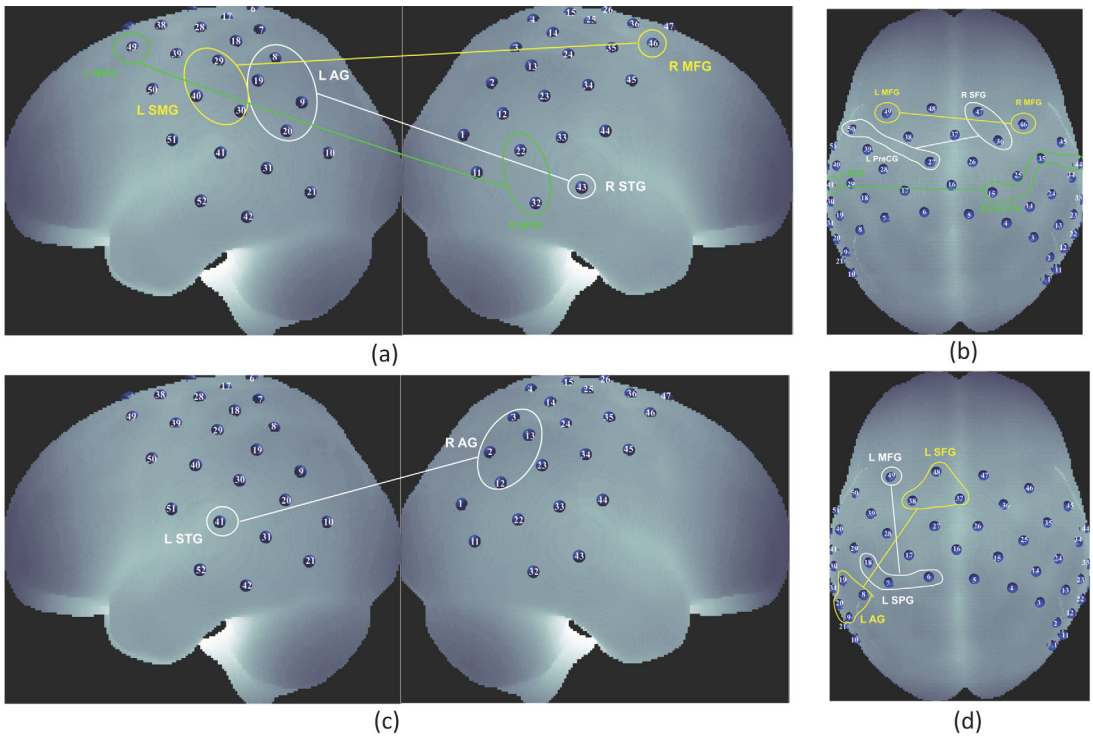

Figure 5. Selected connections as features by using ten-fold cross validation of LASSO for classifiers. Regions are defined according to the table 1. (a) Connections for INDc condition. (b) Connections for BS condition. (c) and (d) Connections for the SUBc condition.

To minimize $L(\boldsymbol{\theta})$, we used an acquisition function F to sample the $L(\boldsymbol{\theta})$, at $\boldsymbol{\theta_i}$.

$$\boldsymbol{\theta_i} = \arg\max_{\boldsymbol{\theta}} F(\boldsymbol{\theta}|\ S_{1:\mathbf{k-1}}).$$

In this equation, F is the acquisition function. In this study, we used expected-improvement criteria as the acquisition function to choose the next set of the hyperparameters for all classifiers. $\boldsymbol{S_{1:k-1}} = [(\boldsymbol{\theta_1},\ C_1), (\boldsymbol{\theta_2}, C_2) \ldots\ldots\ldots (\boldsymbol{\theta_{k-1}}, C_{k-1})]$ is the set of hyperparameters for every run of classifier and validation loss values. k is the number of repetition $1, 2, \ldots.., k-1$. The Bayesian optimization algorithm works as below:

- Finding the next set of hyperparameters by optimizing the acquisition function F on $\boldsymbol{\theta_i} = \arg\max_{\boldsymbol{\theta}}\ F(\boldsymbol{\theta}|\ S_{1:\mathbf{k-1}})$.
- Finding a time point that is possibly noisy $C_k = L(\boldsymbol{\theta_k}) + \epsilon_k$.
- Updating the hyperparameter and validation loss values set $\boldsymbol{S_{1:k}} = [\boldsymbol{S_{1:k-1}}, (\boldsymbol{\theta_k}, C_k)]$.

While performing hyperparameter optimization, we used leave one out cross validation (LOOCV) to generalize the minimum classification error. We applied hyperparameter tuning for the support vector machine (SVM) and linear discriminant analysis (LDA) methods. For SVM, we considered linear, polynomial (deg. 2–10) and radial basis function (RBF) as the kernel with regularization parameter (C) and sigma value (σ) for RBF. We used log transformed values between 10^{-6}–10^{6} for C and σ. For DA, we considered linear, quadratic, diagonal linear, diagonal quadratic, pseudo linear, and pseudo quadratic discriminant types with a linear coefficient threshold (δ) and regularization parameter (γ). For δ, we considered log transformed values between 10^{-6}–10^{6}, and for γ we considered values between 0–1. All these procedures were performed by using MATLAB Statistics and Machine Learning Toolbox (MathWorks, Inc., Natick, Massachusetts).

2.6.5. *Nested cross validation*

After extracting features and creating a feature vector with a size of 40 × 3 for three conditions, we applied a nested cross validation (CV) procedure to optimize hyperparameters and generalize classifier results. In this nested cross validation model, the outer ten-fold CV loop was used to test the generalization of the classification model with the tuned hyperparameters (for SVM, kernel, C and σ for RBF and for DA, discriminant type, δ and γ). The inner loop includes the hyperparameter optimization with a ten-fold CV.

2.6.6. *Statistical analysis of VAS data*

All statistical analyses were performed using SPSS 20.0. For the age and pain threshold comparison, we used paired t-test, and for the comparison of VAS ratings, we performed a 2 × 2 (Group (SSD and HC) × Condition (SUBc and INDc)) ANOVA to find whether there is a statistically significant difference between groups or stimulation. We performed

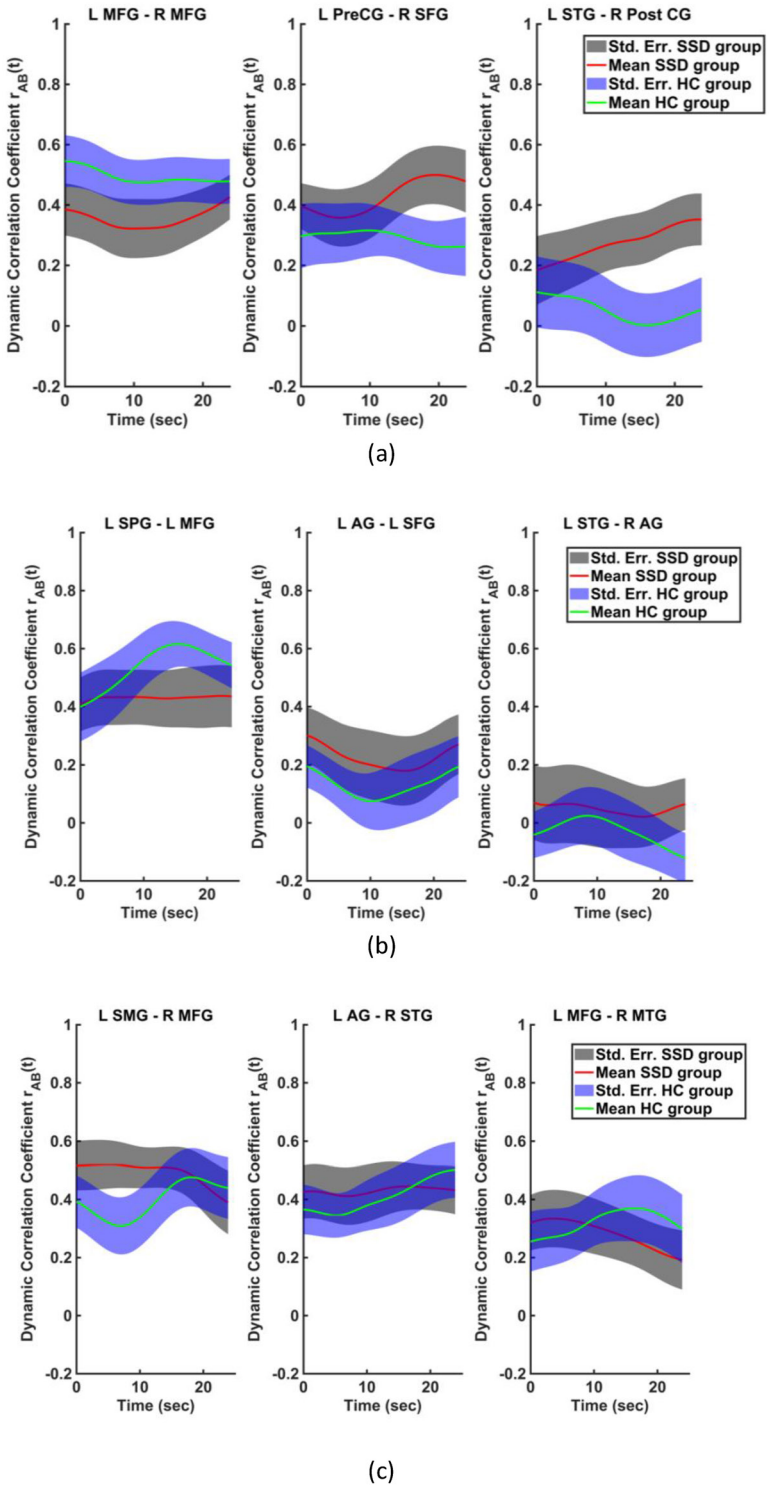

Figure 6. Mean dynamic correlation vector ($r_{AB}(t)$) for (a) the BS condition, (b) SUBc condition (c) INDc condition of both SSD and HC groups. Green: mean.

Pearson's correlation between clinical data and features for every condition.

3. Results

3.1. Clinical data analysis

Demographic and clinical scores are shown in table 2. There was no difference between groups for age (t-val. $= 0.82$, $p = 0.41$) and pain threshold (t-val. $= -0.62$, $p = 0.53$) variables. SSD patients showed significantly higher BDI (t-val. $= 5.38$, $p < 0.001$) than healthy controls. VAS ratings of SUB were 48.59 ± 18.37 for SSD patients and 43.33 ± 16.00 for HC. For INDc, VAS ratings were 68.94 ± 17.74 and 68.80 ± 14.61 for SSD patients and HC respectively. ANOVA results revealed that there was no group difference between SSD and HC groups ($F(1,79) = 0.91$, $p = 0.34$). There was a significant difference between SUBc and INDc ($F(1,79) = 28.79$, $p = 0.00$). Post hoc results using Bonferroni correction

Table 2. Clinical and demographic information of participants. Mean and standard deviation values with *t*-values, 95% confidence interval and *p*-values are shown.

	Somatoform patients ($n = 19$, 7 F,12 M)	Healthy controls ($n = 21$, 8 F,13 M)	*t*-value	95%-CI	*P*-value
Age (years)	43.47 ± 12.59	40.00 ± 13.97	0.82	−5.07–12.02	0.41
Pain threshold (gf mm^{-2})	186.84 ± 22.12	190.47 ± 13.95	−0.62	−15.35–8.08	0.53
BDI	21.25 ± 12.67	5.50 ± 4.57	5.38	9.82–21.67	<0.001[a] $p = 0.000035527$

BDI: Beck depression inventory, CI: confidence interval, gf mm^{-2}: gram force/millimeter square, M: male, F: female. n: number of participants.
[a] $p < 0.001$.
[b] $p < 0.05$.

Table 3. Classification results of experiments after nested cross-validation. Results are shown as mean and standard error.

Condition	Classifier	Training accuracy	Test accuracy	Sensitivity	Specificity	AUC
BS	SVM	0.79 ± 0.01	0.75 ± 0.06	0.86 ± 0.07	0.65 ± 0.13	0.89 ± 0.01
	DA	0.75 ± 0.01	0.72 ± 0.07	0.78 ± 0.11	0.70 ± 0.11	0.90 ± 0.02
SUBc	SVM	0.81 ± 0.01	0.72 ± 0.07	0.75 ± 0.08	0.70 ± 0.11	0.89 ± 0.01
	DA	0.78 ± 0.01	0.75 ± 0.06	0.75 ± 0.08	0.75 ± 0.08	0.88 ± 0.01
INDc	SVM	0.80 ± 0.02	0.82 ± 0.05	0.81 ± 0.07	0.85 ± 0.07	0.92 ± 0.02
	DA	0.79 ± 0.01	0.75 ± 0.07	0.81 ± 0.07	0.65 ± 0.13	0.89 ± 0.01

BS: brush stimulation, SUBc: constant sub-threshold painful stimulation condition, INDc: individual pain threshold stimulation condition. SVM: support vector machine, DA: discriminant analysis. AUC: area under curve.

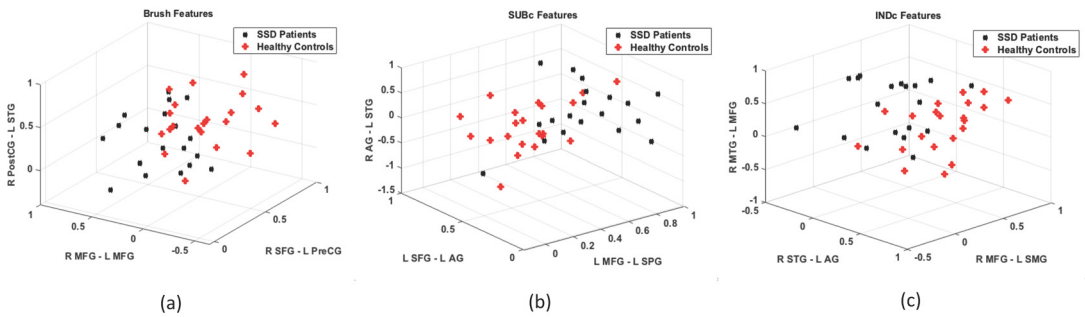

Figure 7. Extracted features from (a) BS condition, (b) SUBc condition (c) INDc condition. Black and red dots represent the mean correlation value of the averaged extracted correlation vector for the related condition of SSD patients and healthy controls respectively.

revealed that INDc caused a higher VAS score than SUBc (mean ± std. dev = 20.99 ± 3.91, 95% CI: 13.20–28.79). There was no interaction between group and stimulation type ($F(1,79) = 0.02, p = 0.894$).

3.2. Classification and hyperparameters optimization results

All classification results with optimum hyperparameters for both classifiers are shown in table 3, the scatter plot of data for every condition is shown in figure 7 and all receiver operating characteristic (ROC) curves related with these classification results are shown in figure 8. For feature vectors of BS condition with an SVM classifier, we found the mean and standard error of training accuracy, test accuracy, sensitivity, specificity and area under curve (AUC) values as 0.79 ± 0.01, 0.75 ± 0.01, 0.86 ± 0.07, 0.65 ± 0.13 and 0.89 ± 0.01 respectively. For the DA classifier, the mean and standard error of training accuracy, test accuracy, sensitivity, specificity and AUC values were 0.75 ± 0.01, 0.72 ± 0.07, 0.78 ± 0.11, 0.70 ± 0.11 and 0.90 ± 0.02, respectively.

For the feature vector of the SUBc condition with an SVM classifier, we found the mean and standard error of training accuracy, test accuracy, sensitivity, specificity and AUC values as 0.81 ± 0.01, 0.72 ± 0.07, 0.75 ± 0.08, 0.70 ± 0.11 and 0.89 ± 0.01, respectively. For the DA classifier, the mean and standard error of training accuracy, test accuracy, sensitivity, specificity and AUC were 0.78 ± 0.01, 0.75 ± 0.06, 0.75 ± 0.08, 0.75 ± 0.08 and 0.88 ± 0.01 respectively.

For the feature vector of the INDc condition with an SVM classifier, the mean and standard error of training accuracy, test accuracy, sensitivity, specificity and AUC was found to be 0.80 ± 0.02, 0.82 ± 0.05, 0.81 ± 0.07, 0.85 ± 0.07 and 0.92 ± 0.02, respectively. For the DA classifier, the mean and standard error of training accuracy, test accuracy, sensitivity, specificity and AUC

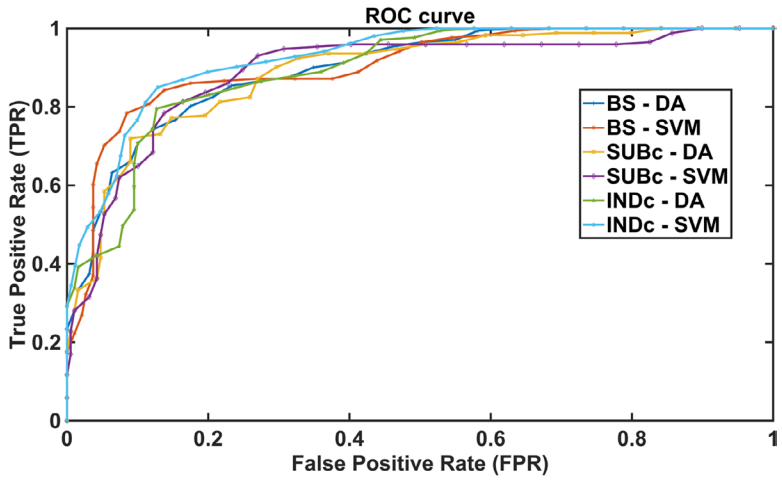

Figure 8. Receiver operating characteristic (ROC) curves for different feature sets and different classifiers.

values were 0.79 ± 0.01, 0.75 ± 0.07, 0.81 ± 0.07, 0.65 ± 0.13 and 0.89 ± 0.01, respectively.

3.3. Correlation between features and psychological features

Among all conditions and all connections, for SUBc there was a significant negative correlation between L SFG—L AG connection and BDI score ($r = -0.33$, $p < 0.05$). None of the features in any condition showed significant correlation with individual pain thresholds.

4. Discussion

In this study, we used fNIRS task-based dFC features to classify SSD. Our objective was to estimate significant biomarker/s from different experiments that accurately discriminate SSD patients and healthy controls. After estimating dynamic functional connectivity-based features using LASSO, we performed hyperparameter-optimized classification using these features. According to our results, we found the most discriminative and accurate biomarkers as connections between Right STG—Left AG, Right MFG—Left SMG and Right MTG—Left MFG as a result of the INDc condition by using SVM.

4.1. Clinical data

We found the SSD group showed significantly higher BDI scores than healthy controls. This is an expected finding. There are several studies that associate depressive symptoms with SSD (Kroenke *et al* 1997, Egger *et al* 1999, Haug *et al* 2004, Bohman *et al* 2010, van Boven *et al* 2011). In addition to this, we could not find any significant difference between pain thresholds and for VAS ratings we could not find any significant difference in group main effect and the INDc condition caused higher VAS scores than SUBc as expected. These findings might suggest that the SSD group might not include any painful disorder.

4.2. Features as biomarkers for different conditions

After dFC estimation and selecting features, we found three discriminative features for every condition. Among these conditions we found the highest accuracy, specificity, AUC and 81% sensitivity for INDc. For INDc, the most discriminative features were found as Right STG—Left AG, Right MFG—Left SMG, Right MTG—Left MFG. Our initial approach for classification was to utilize statistical features HbO_2 response, such as mean and variance that were previously used in BCI studies (Naseer and Hong 2015) and then to perform exactly the same procedure stated above. However, the accuracy results for all three conditions (INDc, SUB, BS) varied between 55%–60%, which were below to be of use as a clinical marker. We therefore focused on the different features to increase the accuracy.

Right STG was found to be a common region in somatoform pain disorder patients for both pain and stress condition (Stoeter *et al* 2007) and also fibromyalgia (Gracely *et al* 2002). In addition to these information, the RSFC study revealed that increased inferior temporal gyrus connectivity was found in SSD patients (Su *et al* 2015). Moreover, the temporal lobe was generally found active in painful stimulation studies in healthy participants (Ploghaus *et al* 2000, Ploghaus *et al* 2001, Bingel *et al* 2002, Godinho *et al* 2006, Moulton *et al* 2011). Its functional role in pain processing is not well known, however some studies revealed that superior temporal gyrus activation might be associated with moral judgements and sadness (Moll *et al* 2002, Habel *et al* 2005).

For subparts of the inferior parietal lobe, RSFC studies revealed that Left AG was found to be significantly higher in SSD patients compared with HC (Song *et al* 2015), and SMG (BA 40) causes difference between SSD and HC (Li *et al* 2016). Left SMG was found to be higher in somatoform pain disorder patients than healthy controls in a painful heat stimulation study (Gundel *et al* 2008) and a recent study

revealed that there is a decreased interhemispheric connectivity in AG and SMG regions for SSD patients (Su *et al* 2016). SMG is also an effective region in an emotional network that may affect pain perception (Sommer *et al* 2010) and also plays an important role in temperature and pressure perception (Mima *et al* 1999, Carlsson *et al* 2000, Tseng *et al* 2010). IPL was also found to be active in pain processing for fibromyalgia patients (Gracely *et al* 2002, Gomez *et al* 2009). Some studies suggest that IPL activation might be related with the attention to body or sensory stimuli (Derbyshire *et al* 1997, Downar *et al* 2000, 2001, Bornhovd *et al* 2002, Seminowicz and Davis 2006).

MFG is an effective region in pain processing and considered as a potential biomarker in nociception (Coghill *et al* 2001, Symonds *et al* 2006, Perlaki *et al* 2015, Aasted *et al* 2016, Jahn *et al* 2016, Ong *et al* 2019), however its contribution to pain processing is not well known. An fMRI study on healthy participants that compares the high and low levels of painful stimulation showed that Left MFG showed higher activation during high levels of pain application than low levels of pain application (Kong *et al* 2010).

4.3. Classification results

Among classification results, we obtained the highest test accuracy (82%) and specificity (85%) with 81% sensitivity from INDc with the SVM classifier. Among all these results, we found the highest sensitivity was 86% for the BS condition by using an SVM classifier. In addition to these results, we found the highest AUC value for INDc with the SVM classifier. Due to these plus signs, we interpreted that our optimum classification results were found by performing the INDc condition with an SVM classifier. A recent RSFC study that includes 53 participants (25 SSD, 28 HC) revealed that the medial prefrontal cortex—anterior cingulate cortex—connection difference between SSD and HC might be used to distinguish with 84% sensitivity and 85% specificity and suggests that this connection can be used as a biomarker (Ou *et al* 2018). When we compared our results with this study, we found the same specificity score and a slightly lower sensitivity score. We thought that this might be due to having less number of samples. Also, due to not having any accuracy result in that study, we could not compare our accuracy and AUC results. Another recent study that uses a symptom self-rating scale (SCL-90) data with machine learning methods showed that SSD can be classified with a 96% accuracy, 90% specificity and 97% sensitivity (Lv *et al* 2018) and another study that proposes to classify a framework for classification of SSD by using SCL-90 data showed that 95% accuracy, 97% sensitivity and 90% specificity (Luo *et al* 2019). However, as we stated above, self-reporting is a subjective approach for diagnosis and can be significantly affected from external factors (Lee *et al* 2018).

Another important finding in this study is that neural markers of BS stimulation discriminated the SSD and HC with a high sensitivity of 86%. A behavioral study by using the Somatic Signal Detection Task (Lloyd *et al* 2008) on SSD patients showed that tactile detection thresholds of SSD patients are significantly lower than control groups (Katzer *et al* 2012). Another study that focused on tactile stimulus perception on fibromyalgia (FM) and somatoform pain disorder (SPD), which is a subtype of SSD, showed that FM and SPD groups showed higher perceptual ratings to tactile stimulation to both their hands (Karst *et al* 2005). These perceptual differences might have neural reflections that can be utilized to discriminate SSD patients and healthy controls.

We also found a notable accuracy in both SUBc and INDc stimulation. Applying painful stimulus to these patients might reveal some differed neural activations compared with HC. The term 'central sensitization' might be an discriminative factor for the diagnosis of SSD patients, which might be a common factor in somatic syndromes (Bourke *et al* 2015). Compared with BS stimulation, INDc shows a notably higher sensitivity, which might show us painful stimulation-based neural markers might be also discriminative factors. An fMRI study focused on painful stimulation response in SSD patients revealed that the SSD group showed augmented prefrontal, temporal and parietal regions with sub-cortical regions such as the thalamus, basal ganglia and also an overactivation in STG, which is a region that we utilized both in SUBc and INDc conditions to classify SSD, was found (Stoeter *et al* 2007). Another fMRI study also revealed that painful stimulation-based neural activity in SMG was observed higher in SSD patients than healthy controls, which we also used in INDc for classification (Gundel *et al* 2008).

Our study also proposed that fNIRS might be a robust tool for the diagnosis of SSD. To our best knowledge, there is only one study that focuses on somatoform pain disorders by using fNIRS (Ren *et al* 2017). In addition this, there are few fNIRS studies that focused on classifying neurological disorders by utilizing machine learning approaches such as ADHD (Monden *et al* 2015, Sutoko *et al* 2019), Alzheimer's (Perpetuini *et al* 2019), traumatic brain injury (Karamzadeh *et al* 2016a, 2016b), depression (Zhu and Mehta 2017), and fibromyalgia (Gokcay *et al* 2018). Classification accuracies with sensitivity and specificity scores showed that fNIRS can be considered as an essential tool, which suggests a neurobiological support to the valid diagnosis of SSD that is phenomenologically diagnosed and for the diagnosis of other psychological disorders (see reviews (Baskak 2018, Ehlis *et al* 2014, Lai *et al* 2017)).

4.4. Correlation results with corresponding biomarkers

Among our features, we obtained a significant negative correlation between BDI scores and the L SFG—L AG connection of SUBc. A previous resting-state fMRI study that focused on sub-regions of L SFG revealed that L AG is strongly associated with anteromedial and dorsolateral parts of SFG (Li *et al* 2013). In addition to this, a recent study that focused on the efficiency of electroconvulsive therapy on depression patients showed that the increased functional connectivity strength of L AG was observed in depression patients after electroconvulsive therapy (Wei *et al* 2018). These findings revealed that the L AG—L SFG relationship might be an effective indicator for depressive symptoms of SSD.

5. Limitations

In the current study, we used fNIRS to demonstrate its efficiency while diagnosing SSD in clinics and classify whether the participant has an SSD or not by using hyper-parameter tuned machine learning approaches. However, there are some points that should be addressed.

Our primary limitation is the number of subjects that participate in this study. While performing machine learning approaches in medicine, using larger samples provides more reliable and robust models. Due to this reason, more extensive research with larger population sizes must be realized.

The second limitation is, while estimating the connections, we had to discard the sub-cortical activities due to being unable to measure deep regions more than 2–3 cm. Our features were estimated by considering only cortical regions. This deprived us to observe some direct connections between regions. We had to estimate the functional connectivity-based features just considering the cortical regions.

Our third limitation was being unable to use short source-detector separation for eliminating skin/scalp blood flow reaction to experimental stimuli from our time series. Due to not having any rule of thumb to remove this effect except using short separation, this effect might be available in our time series.

Finally, our primary aim was to assess the neurobiology of SSD and we therefore excluded subjects with major depressive disorder. Due to high comorbidity of these two disorders, this preference of ours inevitably led to a lower external validity. Our results may not be generalized to all subjects with SSD.

6. Conclusions

In this study, we have shown that after controlling for depressive symptoms, subjects with DSM-5 diagnosis of SSD can be differentiated from healthy control subjects by means of a machine-learning algorithm based on extracted features from estimated dynamic functional connectivity time series as a response to painful stimuli. Our study includes several novel approaches. To our best knowledge, this is the first study that focuses on painful and non-painful stimulation effects together on SSD patients, that proposes biomarkers for SSD by using fNIRS and performs a hyperparameter-optimized classification using these fNIRS-based biomarkers. Previous studies with a similar methodology pointed out that some somatoform disorders, such as somatoform pain disorder or fibromyalgia, may also be associated with altered activity response to painful stimuli. Nevertheless, the sample enrolled in the present study have prominent differences compared to those studies.

According to our findings, the highest accuracy, highest specificity and 90% sensitivity were obtained by features that was derived from task-based dynamic functional connectivity by performing an IND experiment. Right temporal, bilateral middle frontal and left inferior parietal gyri were found as important biomarkers. Although we have shown that this algorithm is capable of categorizing subjects with SSD with acceptable sensitivity and specificity, given that SSD is a phenomenologically diagnosed syndrome, it would be too assertive to suggest fNIRS as a diagnostic tool for this syndrome. Therefore, the present study would rather be evaluated as a pilot study with positive results supporting the validity of the SSD diagnosis in the DSM-5.

Acknowledgments

The authors express their gratitude to the Ankara University BAUM Center for data acquisition and Assoc. Prof. Dr Didem Gökçay from Middle East Technical University for providing the eVF anesthesiometer. We also acknowledge the support, in part, of the Fogarty International Center, United States/NIH Grant (No. D43TW005807—Bora Baskak, MD), during the preparation of this manuscript.

Conflict of interest

The authors declare that there are no conflicts of interest regarding the publication of this paper.

ORCID iDs

Aykut Eken https://orcid.org/0000-0002-7023-7930

References

Aasted C M, Yucel M A, Steele S C, Peng K, Boas D A, Becerra L and Borsook D 2016 Frontal lobe hemodynamic responses to painful stimulation: a potential brain marker of nociception *PLoS One* **11** e0165226

Ambalavanar R, Moritani M, Moutanni A, Gangula P, Yallampalli C and Dessem D 2006 Deep tissue inflammation upregulates neuropeptides and evokes nociceptive behaviors which are modulated by a neuropeptide antagonist *Pain* **120** 53–68

American Psychiatric Association 2013 *Diagnostic and Statistical Manual of Mental Disorders* 5th edn (Washington, DC: American Psychiatric Association)
Andreasen N C 1995 The validation of psychiatric diagnosis: new models and approaches *Am. J. Psychiatry* **152** 161–2
Asano T, Takahashi K A, Fujioka M, Inoue S, Ueshima K, Hirata T and Kubo T 2004 Relationship between postrenal transplant osteonecrosis of the femoral head and gene polymorphisms related to the coagulation and fibrinolytic systems in Japanese subjects *Transplantation* **77** 220–5
Barsky A J, Goodson J D, Lane R S and Cleary P D 1988 The amplification of somatic symptoms *Psychosom. Med.* **50** 510–9
Barsky A J, Orav E J and Bates D W 2005 Somatization increases medical utilization and costs independent of psychiatric and medical comorbidity *Arch. Gen. Psychiatry* **62** 903–10
Baskak B 2018 The place of functional near infrared spectroscopy in psychiatry *Noro Psikiyatr. Ars.* **55** 103–4
Bingel U, Quante M, Knab R, Bromm B, Weiller C and Buchel C 2002 Subcortical structures involved in pain processing: evidence from single-trial fMRI *Pain* **99** 313–21
Bohman H, Jonsson U, Von Knorring A L, Von Knorring L, Paaren A and Olsson G 2010 Somatic symptoms as a marker for severity in adolescent depression *Acta Paediatr.* **99** 1724–30
Bornhovd K, Quante M, Glauche V, Bromm B, Weiller C and Buchel C 2002 Painful stimuli evoke different stimulus-response functions in the amygdala, prefrontal, insula and somatosensory cortex: a single-trial fMRI study *Brain* **125** 1326–36
Bourke J H, Langford R M and White P D 2015 The common link between functional somatic syndromes may be central sensitisation *J. Psychosom. Res.* **78** 228–36
Browning M, Fletcher P and Sharpe M 2011 Can neuroimaging help us to understand and classify somatoform disorders? A systematic and critical review *Psychosom. Med.* **73** 173–84
Callan D, Mills L, Nott C, England R and England S 2014 A tool for classifying individuals with chronic back pain: using multivariate pattern analysis with functional magnetic resonance imaging data *PLoS One* **9** e98007
Carlsson K, Petrovic P, Skare S, Petersson K M and Ingvar M 2000 Tickling expectations: neural processing in anticipation of a sensory stimulus *J. Cogn. Neurosci.* **12** 691–703
Chiarelli A M, Croce P, Merla A and Zappasodi F 2018 Deep learning for hybrid EEG-fNIRS brain-computer interface: application to motor imagery classification *J. Neural Eng.* **15** 036028
Chiarelli A M, Zappasodi F, Di Pompeo F and Merla A 2017 Simultaneous functional near-infrared spectroscopy and electroencephalography for monitoring of human brain activity and oxygenation: a review *Neurophotonics* **4** 041411
Coghill R C, Gilron I and Iadarola M J 2001 Hemispheric lateralization of somatosensory processing *J. Neurophysiol.* **85** 2602–12
Cope M and Delpy D T 1988 System for long-term measurement of cerebral blood and tissue oxygenation on newborn infants by near infra-red transillumination *Med. Biol. Eng. Comput.* **26** 289–94
Davis K D, Flor H, Greely H T, Iannetti G D, Mackey S, Ploner M and Wager T D 2017 Brain imaging tests for chronic pain: medical, legal and ethical issues and recommendations *Nat. Rev. Neurol.* **13** 624–38
Derbyshire S W, Jones A K, Gyulai F, Clark S, Townsend D and Firestone L L 1997 Pain processing during three levels of noxious stimulation produces differential patterns of central activity *Pain* **73** 431–45
Downar J, Crawley A P, Mikulis D J and Davis K D 2000 A multimodal cortical network for the detection of changes in the sensory environment *Nat. Neurosci.* **3** 277–83
Downar J, Crawley A P, Mikulis D J and Davis K D 2001 The effect of task relevance on the cortical response to changes in visual and auditory stimuli: an event-related fMRI study *NeuroImage* **14** 1256–67
Dutta A, Jacob A, Chowdhury S R, Das A and Nitsche M A 2015 EEG-NIRS based assessment of neurovascular coupling during anodal transcranial direct current stimulation—a stroke case series *J. Med. Syst.* **39** 205
Egger H L, Costello E J, Erkanli A and Angold A 1999 Somatic complaints and psychopathology in children and adolescents: stomach aches, musculoskeletal pains, and headaches *J. Am. Acad. Child Adolesc. Psychiatry* **38** 852–60
Ehlis A C, Schneider S, Dresler T and Fallgatter A J 2014 Application of functional near-infrared spectroscopy in psychiatry *NeuroImage* **85** 478–88
Fekete T, Rubin D, Carlson J M and Mujica-Parodi L R 2011 The NIRS Analysis Package: noise reduction and statistical inference *PLoS One* **6** e24322
Garcia-Campayo J, Sanz-Carrillo C, Baringo T and Ceballos C 2001 SPECT scan in somatization disorder patients: an exploratory study of eleven cases *Aust. N. Z. J. Psychiatry* **35** 359–63
Godinho F, Magnin M, Frot M, Perchet C and Garcia-Larrea L 2006 Emotional modulation of pain: is it the sensation or what we recall? *J. Neurosci.* **26** 11454–61
Gokcay D, Eken A and Baltaci S 2019 Binary classification using neural and clinical features: an application in fibromyalgia with likelihood based decision level fusion *IEEE J. Biomed. Health Inform.* **23** 1490–8
Gomez J M, Vilarrasa N, Masdevall C, Pujol J, Solano E, Soler J and Vendrell J 2009 Regulation of bone mineral density in morbidly obese women: a cross-sectional study in two cohorts before and after bypass surgery *Obes. Surg.* **19** 345–50
Gracely R H, Petzke F, Wolf J M and Clauw D J 2002 Functional magnetic resonance imaging evidence of augmented pain processing in fibromyalgia *Arthritis. Rheum.* **46** 1333–43
Gundel H, Valet M, Sorg C, Huber D, Zimmer C, Sprenger T and Tolle T R 2008 Altered cerebral response to noxious heat stimulation in patients with somatoform pain disorder *Pain* **137** 413–21
Habel U, Klein M, Kellermann T, Shah N J and Schneider F 2005 Same or different? Neural correlates of happy and sad mood in healthy males *NeuroImage* **26** 206–14
Hakala M, Karlsson H, Kurki T, Aalto S, Koponen S, Vahlberg T and Niemi P M 2004 Volumes of the caudate nuclei in women with somatization disorder and healthy women *Psychiatry Res.* **131** 71–8
Hakala M, Vahlberg T, Niemi P M and Karlsson H 2006 Brain glucose metabolism and temperament in relation to severe somatization *Psychiatry Clin. Neurosci.* **60** 669–75
Haug T T, Mykletun A and Dahl A A 2004 The association between anxiety, depression, and somatic symptoms in a large population: the HUNT-II study *Psychosom. Med.* **66** 845–51
Hisli N 1998 A study on the validity of the Beck depression inventory *Turk. Psychol. J.* **6** 118–23
Homae F, Watanabe H, Otobe T, Nakano T, Go T, Konishi Y and Taga G 2010 Development of global cortical networks in early infancy *J. Neurosci.* **30** 4877–82
Jablensky A 2016 Psychiatric classifications: validity and utility *World Psychiatry* **15** 26–31
Jahn A, Nee D E, Alexander W H and Brown J W 2016 Distinct regions within medial prefrontal cortex process pain and cognition *J. Neurosci.* **36** 12385–92
Jang K E, Tak S, Jung J, Jang J, Jeong Y and Ye J C 2009 Wavelet minimum description length detrending for near-infrared spectroscopy *J. Biomed. Opt.* **14** 034004
Janssens K A, Oldehinkel A J, Verhulst F C, Hunfeld J A, Ormel J and Rosmalen J G 2012 Symptom-specific associations between low cortisol responses and functional somatic symptoms: the TRAILS study *Psychoneuroendocrinology* **37** 332–40
Karamzadeh N, Amyot F, Kenney K, Anderson A, Chowdhry F, Dashtestani H and Gandjbakhche A H 2016a A machine learning approach to identify functional biomarkers in human prefrontal cortex for individuals with traumatic brain injury using functional near-infrared spectroscopy *Brain Behav.* **6** e00541
Karamzadeh N, Amyot F, Kenney K, Chowdhry F, Anderson A, Chernomordik V and Gandjbakhche A 2016b A machine learning approach to identify functional biomarkers for traumatic brain injury (tbi) using functional near-infrared spectroscopy (fNIRS) *Biomedical Optics* BTh4D.2
Karst M, Rahe-Meyer N, Gueduek A, Hoy L, Borsutzky M and Passie T 2005 Abnormality in the self-monitoring mechanism

in patients with fibromyalgia and somatoform pain disorder *Psychosom. Med.* **67** 111–5
Kassab A, Le Lan J, Tremblay J, Vannasing P, Dehbozorgi M, Pouliot P and Nguyen D K 2018 Multichannel wearable fNIRS-EEG system for long-term clinical monitoring *Hum. Brain Mapp.* **39** 7–23
Katzer A, Oberfeld D, Hiller W, Gerlach A L and Witthoft M 2012 Tactile perceptual processes and their relationship to somatoform disorders *J. Abnorm. Psychol.* **121** 530–43
Koessler L, Maillard L, Benhadid A, Vignal J P, Felblinger J, Vespignani H and Braun M 2009 Automated cortical projection of EEG sensors: anatomical correlation via the international 10–10 system *NeuroImage* **46** 64–72
Kong J, Loggia M L, Zyloney C, Tu P, Laviolette P and Gollub R L 2010 Exploring the brain in pain: activations, deactivations and their relation *Pain* **148** 257–67
Konnopka A, Kaufmann C, Konig H H, Heider D, Wild B, Szecsenyi J and Schaefert R 2013 Association of costs with somatic symptom severity in patients with medically unexplained symptoms *J. Psychosom. Res.* **75** 370–5
Koo B, Lee H G, Nam Y, Kang H, Koh C S, Shin H C and Choi S 2015 A hybrid NIRS-EEG system for self-paced brain computer interface with online motor imagery *J. Neurosci. Methods* **244** 26–32
Kroenke K, Jackson J L and Chamberlin J 1997 Depressive and anxiety disorders in patients presenting with physical complaints: clinical predictors and outcome *Am. J. Med.* **103** 339–47
KuKanich B, Lascelles B D and Papich M G 2005 Assessment of a von Frey device for evaluation of the antinociceptive effects of morphine and its application in pharmacodynamic modeling of morphine in dogs *Am. J. Vet. Res.* **66** 1616–22
Kurlansik S L and Maffei M S 2016 Somatic symptom disorder *Am. Fam. Physician.* **93** 49–54
Lai C Y Y, Ho C S H, Lim C R and Ho R C M 2017 Functional near-infrared spectroscopy in psychiatry *BJPsych Adv.* **23** 324–30
Lee J, Mawla I, Kim J, Loggia M L, Ortiz A, Jung C and Napadow V 2019 Machine learning-based prediction of clinical pain using multimodal neuroimaging and autonomic metrics *Pain* **160** 550–60
Li Q, Xiao Y, Li Y, Li L, Lu N, Xu Z and Yuan Y 2016 Altered regional brain function in the treatment-naive patients with somatic symptom disorder: a resting-state fMRI study *Brain Behav.* **6** e00521
Li W, Qin W, Liu H, Fan L, Wang J, Jiang T and Yu C 2013 Subregions of the human superior frontal gyrus and their connections *NeuroImage* **78** 46–58
Li Z, Liu H, Liao X, Xu J, Liu W, Tian F and Niu H 2015 Dynamic functional connectivity revealed by resting-state functional near-infrared spectroscopy *Biomed. Opt. Express* **6** 2337–52
Linden D E and Fallgatter A J 2009 Neuroimaging in psychiatry: from bench to bedside *Frontiers Hum. Neurosci.* **3** 49
Lloyd D M, Mason L, Brown R J and Poliakoff E 2008 Development of a paradigm for measuring somatic disturbance in clinical populations with medically unexplained symptoms *J. Psychosom. Res.* **64** 21–4
Lopez-Sola M, Woo C W, Pujol J, Deus J, Harrison B J, Monfort J and Wager T D 2017 Towards a neurophysiological signature for fibromyalgia *Pain* **158** 34–47
Lotsch J and Ultsch A 2018 Machine learning in pain research *Pain* **159** 623–30
Luo J, Chen H, Hu Z, Huang H, Wang P, Wang X and Wen C 2019 A new kernel extreme learning machine framework for somatization disorder diagnosis jie *IEEE Access* **7** 45512–25
Lv X, Chen H, Zhang Q, Li X, Huang H and Wang G 2018 An improved bacterial-foraging optimization-based machine learning framework for predicting the severity of somatization disorder *Algorithms* **11** 17
Mano H, Kotecha G, Leibnitz K, Matsubara T, Sprenger C, Nakae A and Seymour B 2018 Classification and characterisation of brain network changes in chronic back pain: a multicenter study *Wellcome Open Res.* **3** 19
Mima T, Sadato N, Yazawa S, Hanakawa T, Fukuyama H, Yonekura Y and Shibasaki H 1999 Brain structures related to active and passive finger movements in man *Brain* **122** 1989–97
Molavi B and Dumont G A 2012 Wavelet-based motion artifact removal for functional near-infrared spectroscopy *Physiol. Meas.* **33** 259–70
Moll J, de Oliveira-Souza R, Bramati I E and Grafman J 2002 Functional networks in emotional moral and nonmoral social judgments *NeuroImage* **16** 696–703
Monden Y, Dan I, Nagashima M, Dan H, Uga M, Ikeda T and Yamagata T 2015 Individual classification of ADHD children by right prefrontal hemodynamic responses during a go/no-go task as assessed by fNIRS *NeuroImage Clin.* **9** 1–12
Montero-Hernandez S, Orihuela-Espina F, Sucar E L, Pinti P, Hamilton A, Burgess P and Tachtsidis I 2018 Estimating Functional Connectivity Symmetry between Oxy- and Deoxy-Haemoglobin: implications for fNIRS connectivity analysis *Algorithms* **11 70**
Moulton E A, Becerra L, Maleki N, Pendse G, Tully S, Hargreaves R and Borsook D 2011 Painful heat reveals hyperexcitability of the temporal pole in interictal and ictal migraine states *Cereb Cortex* **21** 435–48
Naseer N and Hong K S 2015 fNIRS-based brain-computer interfaces: a review *Frontiers Hum. Neurosci.* **9** 3
Niu H, Khadka S, Tian F, Lin Z J, Lu C, Zhu C and Liu H 2011 Resting-state functional connectivity assessed with two diffuse optical tomographic systems *J. Biomed. Opt.* **16** 046006
Okamoto M, Dan H, Sakamoto K, Takeo K, Shimizu K, Kohno S and Dan I 2004 Three-dimensional probabilistic anatomical cranio-cerebral correlation via the international 10–20 system oriented for transcranial functional brain mapping *NeuroImage* **21** 99–111
Oldfield R C 1971 The assessment and analysis of handedness: the edinburgh inventory *Neuropsychologia* **9** 97–113
Ong W Y, Stohler C S and Herr D R 2019 Role of the prefrontal cortex in pain processing *Mol. Neurobiol.* **56** 1137–66
Ou Y, Liu F, Chen J, Pan P, Wu R, Su Q and Guo W 2018 Increased coherence-based regional homogeneity in resting-state patients with first-episode, drug-naive somatization disorder *J. Affect Disord.* **235** 150–4
Peng K, Nguyen D K, Vannasing P, Tremblay J, Lesage F and Pouliot P 2016 Using patient-specific hemodynamic response function in epileptic spike analysis of human epilepsy: a study based on EEG-fNIRS *NeuroImage* **126** 239–55
Perlaki G, Orsi G, Schwarcz A, Bodi P, Plozer E, Biczo K and Janszky J 2015 Pain-related autonomic response is modulated by the medial prefrontal cortex: an ECG-fMRI study in men *J. Neurol. Sci.* **349** 202–8
Perpetuini D, Chiarelli M A, Cardone D, Filippini C, Bucco R, Zito M and Merla A 2019 Complexity of frontal cortex fNIRS can support alzheimer disease diagnosis in memory and visuo-spatial tests *Entropy* **21** 26
Ploghaus A, Narain C, Beckmann C F, Clare S, Bantick S, Wise R and Tracey I 2001 Exacerbation of pain by anxiety is associated with activity in a hippocampal network *J. Neurosci.* **21** 9896–903
Ploghaus A, Tracey I, Clare S, Gati J S, Rawlins J N and Matthews P M 2000 Learning about pain: the neural substrate of the prediction error for aversive events *Proc. Natl Acad. Sci. USA* **97** 9281–6
Ren X, Lu J, Liu X, Shen C, Zhang X, Ma X and Liu P 2017 Decreased prefrontal brain activation during verbal fluency task in patients with somatoform pain disorder: an exploratory multi-channel near-infrared spectroscopy study *Prog. Neuropsychopharmacol. Biol. Psychiatry* **78** 153–60
Robinson M E, O'Shea A M, Craggs J G, Price D D, Letzen J E and Staud R 2015 Comparison of machine classification algorithms for fibromyalgia: neuroimages versus self-report *J. Pain* **16** 472–7
Rodriguez-Raecke R, Ihle K, Ritter C, Muhtz C, Otte C and May A 2014 Neuronal differences between chronic low back pain and depression regarding long-term habituation to pain *Eur. J. Pain* **18** 701–11

Rolfe P 2000 In vivo near-infrared spectroscopy *Annu. Rev. Biomed. Eng.* **2** 715–54
Sakoglu U, Pearlson G D, Kiehl K A, Wang Y M, Michael A M and Calhoun V D 2010 A method for evaluating dynamic functional network connectivity and task-modulation: application to schizophrenia *MAGMA* **23** 351–66
Scarapicchia V, Brown C, Mayo C and Gawryluk J R 2017 Functional magnetic resonance imaging and functional near-infrared spectroscopy: insights from combined recording studies *Frontiers Hum. Neurosci.* **11** 419
Seminowicz D A and Davis K D 2006 Cortical responses to pain in healthy individuals depends on pain catastrophizing *Pain* **120** 297–306
Shattuck D W, Mirza M, Adisetiyo V, Hojatkashani C, Salamon G, Narr K L and Toga A W 2008 Construction of a 3D probabilistic atlas of human cortical structures *NeuroImage* **39** 1064–80
Sommer M, Sodian B, Dohnel K, Schwerdtner J, Meinhardt J and Hajak G 2010 In psychopathic patients emotion attribution modulates activity in outcome-related brain areas *Psychiatry Res.* **182** 88–95
Song Y, Su Q, Jiang M, Liu F, Yao D, Dai Y and Guo W 2015 Abnormal regional homogeneity and its correlations with personality in first-episode, treatment-naive somatization disorder *Int. J. Psychophysiol.* **97** 108–12
Stoeter P, Bauermann T, Nickel R, Corluka L, Gawehn J, Vucurevic G and Egle U T 2007 Cerebral activation in patients with somatoform pain disorder exposed to pain and stress: an fMRI study *NeuroImage* **36** 418–30
Strangman G, Culver J P, Thompson J H and Boas D A 2002 A quantitative comparison of simultaneous BOLD fMRI and NIRS recordings during functional brain activation *NeuroImage* **17** 719–31
Strigo I A, Simmons A N, Matthews S C, Craig A D and Paulus M P 2008 Association of major depressive disorder with altered functional brain response during anticipation and processing of heat pain *Arch. Gen. Psychiatry* **65** 1275–84
Su Q, Yao D, Jiang M, Liu F, Jiang J, Xu C and Guo W 2014 Dissociation of regional activity in default mode network in medication-naive, first-episode somatization disorder *PLoS One* **9** e99273
Su Q, Yao D, Jiang M, Liu F, Jiang J, Xu C and Guo W 2015 Increased functional connectivity strength of right inferior temporal gyrus in first-episode, drug-naive somatization disorder *Aust. N. Z. J. Psychiatry* **49** 74–81
Su Q, Yao D, Jiang M, Liu F, Long L, Dai Y and Guo W 2016 Decreased interhemispheric functional connectivity in insula and angular gyrus/supramarginal gyrus: significant findings in first-episode, drug-naive somatization disorder *Psychiatry Res. Neuroimaging* **248** 48–54
Sundermann B, Burgmer M, Pogatzki-Zahn E, Gaubitz M, Stuber C, Wessolleck E and Pfleiderer B 2014 Diagnostic classification based on functional connectivity in chronic pain: model optimization in fibromyalgia and rheumatoid arthritis *Acad. Radiol.* **21** 369–77
Sutoko S, Monden Y, Tokuda T, Ikeda T, Nagashima M, Kiguchi M and Dan I 2019 Distinct Methylphenidate-evoked response measured using functional near-infrared spectroscopy during Go/No-Go task as a supporting differential diagnostic tool between attention-deficit/hyperactivity disorder and autism spectrum disorder comorbid children *Frontiers Hum. Neurosci.* **13** 7
Symonds L L, Gordon N S, Bixby J C and Mande M M 2006 Right-lateralized pain processing in the human cortex: an FMRI study *J. Neurophysiol.* **95** 3823–30
Takizawa R, Kasai K, Kawakubo Y, Marumo K, Kawasaki S, Yamasue H and Fukuda M 2008 Reduced frontopolar activation during verbal fluency task in schizophrenia: a multi-channel near-infrared spectroscopy study *Schizophr. Res.* **99** 250–62
Tena B, Escobar B, Arguis M J, Cantero C, Rios J and Gomar C 2012 Reproducibility of Electronic Von Frey and Von Frey monofilaments testing *Clin. J. Pain* **28** 318–23
Tessner K D, Walker E F, Hochman K and Hamann S 2006 Cortisol responses of healthy volunteers undergoing magnetic resonance imaging *Hum. Brain Mapp.* **27** 889–95
Tibshirani R 1996 Regression shrinkage and selection via the lasso *J. R. Stat. Soc.* B **58** 267–88
Tseng P, Hsu T Y, Muggleton N G, Tzeng O J, Hung D L and Juan C H 2010 Posterior parietal cortex mediates encoding and maintenance processes in change blindness *Neuropsychologia* **48** 1063–70
van Boven K, Lucassen P, van Ravesteijn H, olde Hartman T, Bor H, van Weel-Baumgarten E and van Weel C 2011 Do unexplained symptoms predict anxiety or depression? Ten-year data from a practice-based research network *Br. J. Gen. Pract.* **61** e316–25
Vivancos G G, Verri W A Jr, Cunha T M, Schivo I R, Parada C A, Cunha F Q and Ferreira S H 2004 An electronic pressure-meter nociception paw test for rats *Braz J. Med. Biol. Res.* **37** 391–9
Vossen H G, van Os J, Hermens H and Lousberg R 2006 Evidence that trait-anxiety and trait-depression differentially moderate cortical processing of pain *Clin. J. Pain* **22** 725–9
Wei Q, Bai T, Chen Y, Ji G, Hu X, Xie W and Tian Y 2018 The changes of functional connectivity strength in electroconvulsive therapy for depression: a longitudinal study *Frontiers Neurosci.* **12** 661
Yoshino A, Okamoto Y, Kunisato Y, Yoshimura S, Jinnin R, Hayashi Y and Yamawaki S 2014 Distinctive spontaneous regional neural activity in patients with somatoform pain disorder: a preliminary resting-state fMRI study *Psychiatry Res.* **221** 246–8
Zhang Y J, Lu C M, Biswal B B, Zang Y F, Peng D L and Zhu C Z 2010 Detecting resting-state functional connectivity in the language system using functional near-infrared spectroscopy *J. Biomed. Opt.* **15** 047003
Zhu Y and Mehta M S R K 2017 Machine learning approach on frontal lobe activity to assess depression in adults: implications for rehabilitation outcomes *2017 Int. Symp. on Wearable Robotics and Rehabilitation* pp 1–2
Zou H and Hastie T 2005 Regularization and variable selection via the elastic net *J. R. Stat. Soc.* B **67** 301–20